Published in final edited form as:

J Am Chem Soc. 2021 March 10; 143(9): 3295–3299. doi:10.1021/jacs.0c13470.

Structural Characterization of the $[CuOR]^{2+}$ Core

V. Mahesh Krishnan[#], **Dimitar Y. Shopov**[#], **Caitlin J. Bouchey**, **Wilson D. Bailey**
Department of Chemistry, Washington University in St. Louis, St. Louis, Missouri 63130-4899, United States;

Riffat Parveen, **Bess Vlaisavljevich**
University of South Dakota, Vermillion, South Dakota 57069, United States;

William B. Tolman
Department of Chemistry, Washington University in St. Louis, St. Louis, Missouri 63130-4899, United States;

[#] These authors contributed equally to this work.

Abstract

Formal Cu(III) complexes bearing an oxygen-based auxiliary ligand ($[CuOR]^{2+}$, R = H or CH_2CF_3) were stabilized by modulating the donor character of supporting ligand L^Y (L^Y = 4-Y, *N*,*N*′-bis(2,6-diisopropylphenyl)-2,6-pyridinedicarboxamide, Y = H or OMe) and/or the basicity of the auxiliary ligand, enabling the first characterization of these typically highly reactive cores by NMR spectroscopy and X-ray crystallography. Enhanced lifetimes in solution and slowed rates of PCET with a phenol substrate were observed. NMR spectra corroborate the $S = 0$ ground states of the complexes, and X-ray structures reveal shortened Cu–ligand bond distances that match well with theory.

Understanding the molecular structures, spectroscopic properties, and reactivity of copper–oxygen complexes[1–5] is important for gaining insight into the mechanisms by which copper enzymes and other catalysts function.[6,7] Among the various complexes studied, those comprising the $[CuOH]^{2+}$ core supported by dicarboxamide ligands (Figure 1)[8–14] are notably reactive, attacking C–H and O–H bonds via proton-coupled electron transfer (PCET) processes and undergoing electron transfer at high rates (cf. the rate constant for the reaction of L^HCuOH with 1,2-dihydroanthracene 50 M^{-1} s^{-1} at −25 °C;[9] electron-transfer self-

Corresponding Authors: **Bess Vlaisavljevich** – University of South Dakota, Vermillion, South Dakota 57069, United States; bess.vlaisavljevich@usd.edu, **William B. Tolman** – Department of Chemistry, Washington University in St. Louis, St. Louis, Missouri 63130-4899, United States; wbtolman@wustl.edu.

Complete contact information is available at: https://pubs.acs.org/10.1021/jacs.0c13470

Supporting Information
The Supporting Information is available free of charge at https://pubs.acs.org/doi/10.1021/jacs.0c13470.
DFT structural coordinate file (XYZ)
Experimental details and figures (PDF)

Accession Codes
CCDC 2053118–2053123 contain the supplementary crystallographic data for this paper. These data can be obtained free of charge via www.ccdc.cam.ac.uk/data_request/cif, or by emailing data_request@ccdc.cam.ac.uk, or by contacting The Cambridge Crystallographic Data Centre, 12 Union Road, Cambridge CB2 1EZ, UK; fax: +44 1223 336033.

The authors declare no competing financial interest.

exchange rate constant ~10^4 M^{-1} s^{-1} at −88 °C[13]). The formulations of the complexes are supported by UV–vis spectroscopy (diagnostic absorptions with ligand-to-metal charge-transfer (LMCT) character), EPR silence, resonance Raman spectroscopy (ν_{Cu-O} ≈ 630 cm^{-1}),[13] EXAFS (avg Cu–N,O ≈ 0.1 Å shorter than for the $[Cu^{II}OH]^+$ precursor),[8] and theory.[8,15]

Perturbations of the $[CuOH]^{2+}$ core have been effected by the installation of remote substituents on the flanking aryl rings ($L^{X}CuOH$, Figure 1).[11,12] These perturbations are reflected by shifts in the LMCT energies (lower), redox potentials (higher), basicities (lower), and PCET reaction rates (faster) that may be rationalized by electron withdrawal by the X groups. Changing the pyridyl group to a piperidine ($L^{pip}CuOH$) has the opposite effects, attributed to greater electron donation by the amine donor. In no case has a complex with the $[CuOH]^{2+}$ core been structurally defined by X-ray crystallography, in large part due to its high reactivity and poor thermal stability ($t_{1/2}$ ≈ minutes at −80 °C in THF). These characteristics and the fact that decomposition yields paramagnetic Cu(II) species have also inhibited efforts to obtain NMR spectra that would be useful in confirming the proposed S = 0 ground state. Significantly slower reactions and greater stability were observed for the LCuZ derivatives (Z = halide[8,16] or carboxylate[17]) featuring a less-basic X-type reactive moiety, of which the halide complexes were characterized recently by X-ray diffraction and NMR spectroscopy.[16] Inspired by that success, we hypothesized that more complete characterization of the $[CuOH]^{2+}$ core might be attained if its stability could be enhanced. Toward this end, we targeted two modifications: the placement of an electron-donating *para*-methoxy pyridyl group (Y = OMe; L^{OMe}) and the use of a less-basic alkoxide moiety ($CF_3CH_2O^-$). On the basis of previous work,[9,11,12] we hypothesized that these changes would enhance the solution stability, thereby facilitating handling and characterization. We now report the confirmation of these hypotheses through the synthesis of the targeted derivatives and their characterization by X-ray crystallography and NMR spectroscopy, which with comparison to results from theory provides new insights into the molecular and electronic structures of complexes with $[CuOH]^{2+}$ and $[CuOCH_2CF_3]^{2+}$ cores.

The reaction of proligand H_2L^{OMe} with $Cu(OTf)_2$ in the presence of NaOMe and CH_3CN led to the isolation of key precursor $L^{OMe}Cu(CH_3CN)$ (77%), which upon treatment with NBu_4OH led to $[NBu_4][L^{OMe}CuOH]$ (76%). $[NBu_4]$-$[L^{Y}CuOCH_2CF_3]$ (Y = H or OMe) complexes were obtained from the respective hydroxide precursors via protonolysis with $HOCH_2CF_3$. The complexes $L^{OMe}Cu(CH_3CN)$, $[NBu_4]$-$[L^{OMe}CuOH]$, and $[NBu_4]$ $[L^{Y}CuOCH_2CF_3]$ (Y = H or OMe) were characterized by UV–vis and X-band EPR spectroscopy, CHN analysis, and X-ray crystallography (SI). The complexes feature a slightly distorted square-planar geometry (τ_4 = 0.15–0.22)[18] with Cu–N,O bond distances typical for such Cu(II) species (Figures S43–S45; Table 1) and characteristic S = 1/2 rhombic signals with Cu and N hyperfine patterns in EPR spectra (Figures S7–S9).

The expected electronic perturbations of the L^{OMe} and $-OCH_2CF_3$ moieties are reflected in cyclic voltammograms (THF, 0.2 M Bu_4NPF_6), which contain quasi-reversible waves associated with $[CuOR]^{2+}/[CuOR]^+$ couples (Table 2). Good reversibility of the waves for the $-OCH_2CF_3$ complexes is apparent at scan rates as slow as 10 mV/s (Figure S20), consistent with low reactivity for the oxidized species (*vide infra*). A more modest

enhancement of reversibility is seen for $[NBu_4][L^{OMe}\ CuOH]$ relative to the analog supported by L^H (Figure S18).[5] The replacement of −OH with $-OCH_2CF_3$ shifts the $E_{1/2}$ by +0.191 V on average, whereas the alteration of L^Y had a lesser effect, with an average difference of only −0.049 V induced by the introduction of the *p*-OMe substituent.

The chemical oxidation of $[NBu_4][L^{OMe}\ CuOH]$ or $[NBu_4]$-$[L^YCuOCH_2CF_3]$ (Y = H or OMe) was performed by adding 1 equiv of $FcBAr^F{}_4$ or $AcFcBArF_4$, respectively, in THF (−80 °C) or in 1,2-difluorobenzene (DFB, −25 °C). Immediate color changes (deep violet or blue) and intense electronic absorption features (Figure 2) diagnostic of the formation of $[CuOH]^{2+}$ and $[CuOCH_2CF_3]^{2+}$ cores were observed, and reversible one-electron processes were confirmed through titrations and the sequential cyclic additions of oxidant and decamethylferrocene (Figures S22–S27).[13] TDDFT UV–vis transitions exhibit λ_{max} values in agreement with experiment that are predominantly HOMO to LUMO (Figure 2) and shift from 546.1 and 537.1 nm in L^HCuOH and $L^{OMe}CuOH$ to 578. 7 and 573. 6 nm in $L^HCuOCH_2CF_3$ and $L^{OMe}CuOCH_2CF_3$, respectively, as a result of the stabilization of the LUMO (Table S4, Figures S50–S58). Also in agreement with experiment (and precedent[17a]), additional transitions with partial HOMO-to-LUMO character contribute at longer wavelengths to the spectra for the $-OCH_2CF_3$ complexes. Resonance Raman spectra of frozen solutions (λ_{ex} = 561 nm) of all L^YCuOR complexes contain a signal at ~635 cm^{-1} that we assign as ν_{Cu-OR} by analogy to data acquired for L^HCuOH and theory (Figures S45–S49 and S59, Table S15).[13]

To evaluate how ligand variation influences stability and reactivity, we compared the reactions of L^YCuOH and $L^YCuOCH_2CF_3$ (Y = H or OMe) with 2,4,6-tri-*tert*-butylphenol ($^{ttb}PhOH$) to yield the stable phenoxyl radical.[11,19,20] Second-order rate constants were measured using either 1 equiv (L^YCuOH) or 50 equiv ($L^YCuOCH_2CF_3$) of $^{ttb}PhOH$ at −25 °C in DFB (Table 2). The data show significantly higher reactivity for the hydroxide complexes (≳5000-fold), a difference that may be attributed to the higher basicity of the −OH vs $-OCH_2CF_3$ moieties and/or steric inhibition for the latter. Modest decreases in the rate constants for the cases where Y = OMe at parity for −OR may be rationalized by stabilization of the $[CuOR]^{2+}$ core by the electron-donating methoxide substituent. Monitoring the room-temperature decays of the four $[CuOR]^{2+}$ species in the absence of substrate in THF and DFB revealed complicated kinetic traces, but trends in the overall lifetimes paralleled the $^{ttb}PhOH$ reactivity trends (SI; cf. $t_{1/2} \approx 4$ h vs <1 h for $L^{OMe}CuOCH_2CF_3$ vs LCuOH in DFB).

The enhanced stability of the new complexes led us to attempt characterization by X-ray crystallography. We discovered that the complex prepared by the treatment of $[NBu_4]$ $[L^{OMe}CuOH]$ with $FcBAr^F{}_4$ in DFB could be isolated as suitable deep-purple crystals via the layered diffusion of pentane at −30 °C. Similar attempts with $[NBu_4][L^YCuOCH_2CF_3]$ (Y = H or OMe) failed to give suitable crystals, likely in part due to the formation of highly intractable viscous residues containing $[NBu_4][BAr^F{}_4]$. To circumvent this issue, we employed reactants that would yield insoluble inorganic salts as byproducts. Thus, we reacted $LCu-(CH_3CN)^4$ and $L^{OMe}Cu(CH_3CN)$ with $NaOCH_2CF_3$ and then oxidized the resulting crude materials with $AcFcSbF_6$ in CH_2Cl_2 or DFB. After the removal of a light-

colored precipitate (presumably $NaSbF_6$), suitable crystals of the oxidized products were obtained at −30 °C.

Representations of the X-ray structures of $L^{OMe}CuOH$ and $L^{OMe}CuOCH_2CF_3$ (Figure 3) as well as $L^{H}CuOCH_2CF_3$ (Figure S42) show similar square-planar geometries compared to their $[CuOR]^+$ progenitors (τ_4 = 0.11–0.15), but they are neutral species as expected for one-electron oxidation products. Comparison of metal–ligand bond distances between the oxidized and reduced forms (Table 1) indicates in all but one case shortening upon oxidation, by as much as 0.127 Å. The average Cu–N/O bond contraction in $L^{OMe}CuOH$, 0.102 Å, is in excellent agreement with previously reported EXAFS analyses of $L^{H}CuOH$ (0.1 Å).[8] The trifluoroethoxides show somewhat less contraction and in $L^{OMe}CuOCH_2CF_3$ the Cu–O bond even lengthens slightly, by 0.011 Å, but disorder in the trifluoroethoxide ligand imparts an inherent inaccuracy to the O atom's position. Gas-phase geometry optimizations (SI) for the $S = 0$ ground states of the oxidized species are in excellent agreement with the experimentally determined values (*theory* in Table 1). Overall, the bond length differences between the precursor and oxidation products are consistent with the loss of an electron from orbitals spanning the Cu center and/or its immediate environment, as reported for less-reactive complexes LCuZ (Z = F, Cl, Br).[16] Furthermore, the lack of significant structural changes associated with this redox event agrees with the low reorganization energy of 0.95 eV previously measured for the $[L^{H}CuOH]^-/L^{H}CuOH$ couple.[14]

While theoretical calculations support a closed-shell $S = 0$ ground state for the $[CuOH]^{2+}$ core (Table S5),[8] the only experimental corroboration has come from a dearth of signal in the X-band EPR spectrum, an observation consistent with either the $S = 0$ or $S = 1$ ground state. Acquiring NMR spectra, which would distinguish the two spin states, presents challenges due to the formation of paramagnetic Cu(II) decay species. We were nonetheless able to observe sharp peaks in the diamagnetic region of ^1H NMR spectra for both $L^{Y}CuOH$ species in 1,2-dichlorobenzene-d_4 at −15 °C (Figure S28–S29), although broadening due to decomposition was evident for Y = H. The ^1H NMR spectrum of the more robust complex $L^{H}CuOCH_2CF_3$ in THF-d_8 at −80 °C (Figure S30) displayed negligible broadening, but some resonances were obscured by solvent/byproduct signals. Since $L^{OMe}CuOCH_2CF_3$ could be isolated in neat form as a crystalline solid, NMR spectra of isolated material were collected (CD_2Cl_2, −15 °C), and all expected ^1H NMR resonances and J couplings (Figure 4) as well as $^{13}C\{^1H\}$ NMR peaks (Figure S32) were observed. The sharpness of the observed ^1H and $^{13}C\{^1H\}$ NMR features in the diamagnetic chemical shift region confirms an $S = 0$ ground state, in agreement with predictions.[8]

In conclusion, we prepared and characterized a new set of complexes with $[CuOR]^{+/2+}$ cores using a modified supporting ligand and/or core (R = CH_2CF_3). Both changes attenuate the PCET reactivity of the oxidized state, the former by lowering its oxidizing potential and the latter by lowering the basicity of the proton-accepting site. While each modification has the opposite effect on the opposite property (e.g., the less-basic proton acceptor also leads to a more oxidizing species), the dominant impact is on electronics for the supporting ligand and basicity for the core, in line with previously observed reactivity trends and demonstrating how PCET reactivity can be tuned. These stabilization effects were sufficient to permit, for

the first time, the successful characterization of complexes with $[CuOR]^{2+}$ cores by X-ray crystallography and NMR spectroscopy. These data are consistent with several predictions made about $L^{H}CuOH$, in particular, the conservation of geometry with minimal reorganization upon oxidation,[14] the EXAFS-derived contraction of Cu–L bonds by ~0.1 Å on oxidation,[8] the calculated geometries, and the diamagnetic $S = 0$ ground state.[8] To the best of our knowledge, the complexes with R = CH_2CF_3 are the first alkoxo analogs bearing the formal Cu(III) oxidation state, and with the discovery that they share many similarities with their hydroxide counterparts, including PCET reactivity with phenols, the potential for steric and electronic tuning that is unavailable with hydroxide makes this class of compounds promising for further research into the bond-activation properties of high-valent copper species.

Supplementary Material

Refer to Web version on PubMed Central for supplementary material.

ACKNOWLEDGMENTS

We thank the National Institutes of Health (GM 47365) for financial support. X-ray diffraction data were collected using diffractometers acquired through NSF-MRI award no. CHE-1827756. Computations were performed on high performance computing systems at the University of South Dakota, funded by NSF award no. OAC-1626516.

REFERENCES

(1). Mirica LM; Ottenwaelder X; Stack TDP Sructure and Spectroscopy of Copper-Dioxygen Complexes. Chem. Rev 2004, 104, 1013–1045. [PubMed: 14871148]

(2). Lewis EA; Tolman WB Reactivity of Copper-Dioxygen Systems. Chem. Rev 2004, 104, 1047–1076. [PubMed: 14871149]

(3). Elwell CE; Gagnon NL; Neisen BD; Dhar D; Spaeth AD; Yee GM; Tolman WB Copper–Oxygen Complexes Revisited: Structures, Spectroscopy, and Reactivity. Chem. Rev 2017, 117, 2059–2107. [PubMed: 28103018]

(4). Quist DA; Diaz DE; Liu JJ; Karlin KD Activation of dioxygen by copper metalloproteins and insights from model complexes. JBIC, J. Biol. Inorg. Chem 2017, 22, 253–288. [PubMed: 27921179]

(5). Liu JJ; Diaz DE; Quist DA; Karlin KD Copper(I)-Dioxygen Adducts and Copper Enzyme Mechanisms. Isr. J. Chem 2016, 56, 738–755.

(6). (a)Solomon EI; Heppner DE; Johnston EM; Ginsbach JW; Cirera J; Qayyum M; Kieber-Emmons MT; Kjaergaard CH; Hadt RG; Tian L Copper Active Sites in Biology. Chem. Rev 2014, 114, 3659–3853. [PubMed: 24588098] (b)Ciano L; Davies GJ; Tolman WB; Walton PH Bracing copper for the catalytic oxidation of C–H bonds. Nature Catal. 2018, 1, 571–577.

(7). Trammell R; Rajabimoghadam K; Garcia-Bosch I Copper-Promoted Functionalization of Organic Molecules: from Biologically Relevant Cu/O_2 Model Systems to Organometallic Transformations. Chem. Rev 2019, 119, 2954–3031. [PubMed: 30698952]

(8). Donoghue PJ; Tehranchi J; Cramer CJ; Sarangi R; Solomon EI; Tolman WB Rapid C–H Bond Activation by a Monocopper(III)–Hydroxide Complex. J. Am. Chem. Soc 2011, 133, 17602–17605. [PubMed: 22004091]

(9). Dhar D; Tolman WB Hydrogen Atom Abstraction from Hydrocarbons by a Copper(III)-Hydroxide Complex. J. Am. Chem. Soc 2015, 137, 1322–1329. [PubMed: 25581555]

(10). Gagnon N; Tolman WB $[CuO]^{+}$ and $[CuOH]^{2+}$ complexes: intermediates in oxidation catalysis? Acc. Chem. Res 2015, 48, 2126–31. [PubMed: 26075312]

(11). Dhar D; Yee GM; Spaeth AD; Boyce DW; Zhang H; Dereli B; Cramer CJ; Tolman WB Perturbing the Copper(III)–Hydroxide Unit through Ligand Structural Variation. J. Am. Chem. Soc 2016, 138, 356–368. [PubMed: 26693733]

(12). Dhar D; Yee GM; Markle TF; Mayer JM; Tolman WB Reactivity of the copper(III)-hydroxide unit with phenols. Chem. Sci 2017, 8, 1075–1085. [PubMed: 28572905]

(13). Spaeth AD; Gagnon NL; Dhar D; Yee GM; Tolman WB Determination of the Cu(III)–OH Bond Distance by Resonance Raman Spectroscopy Using a Normalized Version of Badger's Rule. J. Am. Chem. Soc 2017, 139, 4477–4485. [PubMed: 28319386]

(14). Zerk TJ; Saouma CT; Mayer JM; Tolman WB Low Reorganization Energy for Electron Self-Exchange by a Formally Copper(III,II) Redox Couple. Inorg. Chem 2019, 58, 14151–14158. [PubMed: 31577145]

(15). Mandal M; Elwell CE; Bouchey CJ; Zerk TJ; Tolman WB; Cramer CJ Mechanisms for Hydrogen-Atom Abstraction by Mononuclear Copper(III) Cores: Hydrogen-Atom Transfer or Concerted Proton-Coupled Electron Transfer? J. Am. Chem. Soc 2019, 141, 17236–17244. [PubMed: 31617707]

(16). Bower JK; Cypcar AD; Henriquez B; Stieber SCE; Zhang S C(sp3)-H Fluorination with a Copper(II)/(III) Redox Couple. J. Am. Chem. Soc 2020, 142, 8514–8521. [PubMed: 32275410]

(17). (a)Elwell CE; Mandal M; Bouchey CJ; Que L Jr.; Cramer CJ; Tolman WB Carboxylate Structural Effects on the Properties and Proton-Coupled Electron Transfer Reactivity of $[CuO_2CR]^{2+}$ Cores. Inorg. Chem 2019, 58, 15872–15879. [PubMed: 31710477] (b)Unjaroen D; Gericke R; Lovisari M; Nelis D; Mondal P; Pirovano P; Twamley B; Farquhar ER; McDonald AR High-Valent d(7) Ni(III) versus d(8) Cu(III) Oxidants in PCET. Inorg. Chem 2019, 58, 16838–16848. [PubMed: 31804808]

(18). Yang L; Powell D; Houser R Structural variation in copper(I) complexes with pyridylmethylamide ligands: structural analysis with a new four-coordinate geometry index, t4. Dalton Trans. 2007, 955–964. [PubMed: 17308676]

(19). Porter TR; Capitao D; Kaminsky W; Qian Z; Mayer JM Synthesis, Radical Reactivity, and Thermochemistry of Monomeric Cu(II) Alkoxide Complexes Relevant to Cu/Radical Alcohol Oxidation Catalysis. Inorg. Chem 2016, 55, 5467–5475. [PubMed: 27171230]

(20). Manner VW; Markle TF; Freudenthal JH; Roth JP; Mayer JM The First Crystal Structure of a Monomeric Phenoxyl Radical: 2,4,6-Tri-tert-butylphenoxyl Radical. Chem. Commun 2008, 256–258.

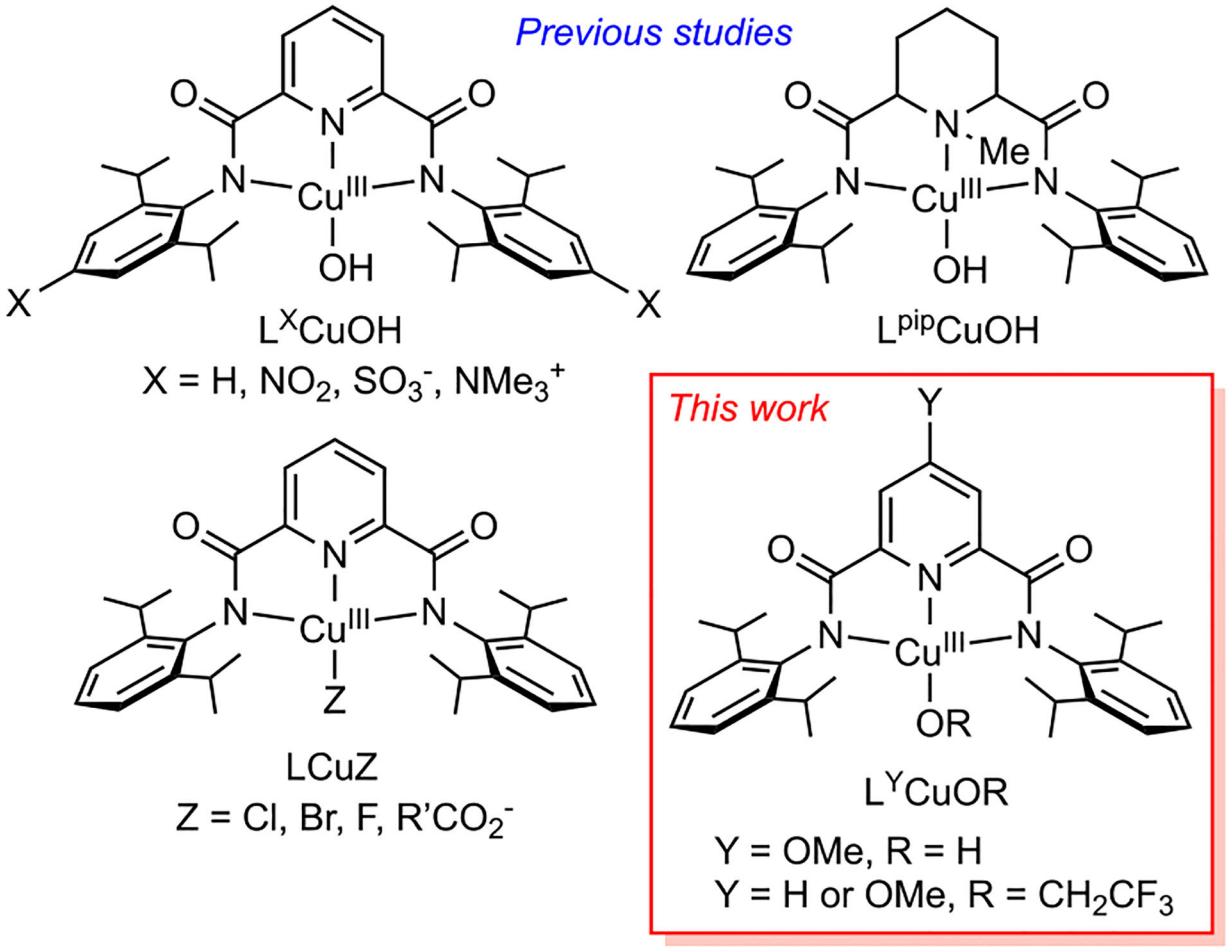

Figure 1.

Complexes studied previously and the compounds that comprise the focus of this work. R′ = Me or aryl groups.

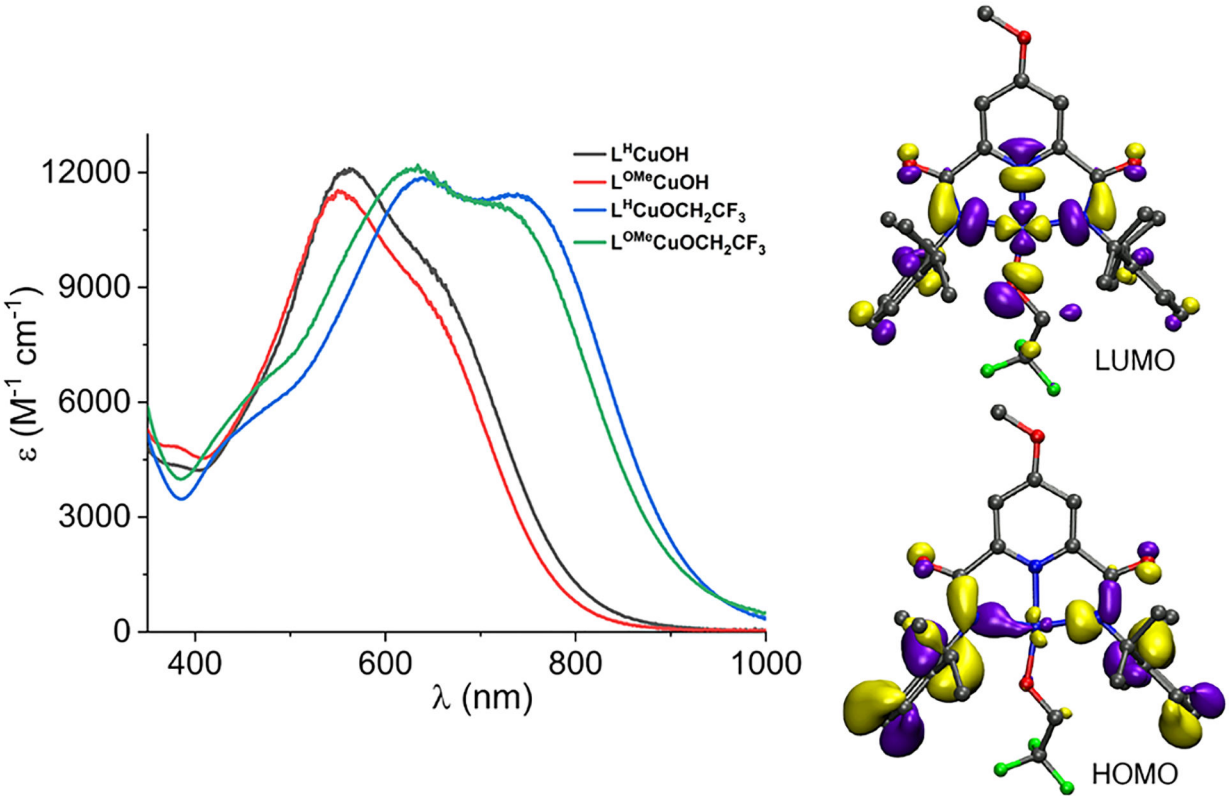

Figure 2.

(Left) UV–visible absorption spectra of the indicated compounds in DFB at −25 °C. (Right) Orbitals for $L^{OMe}CuOCH_2CF_3$ plotted with an isovalue of 0.04 au from the B98 functional.

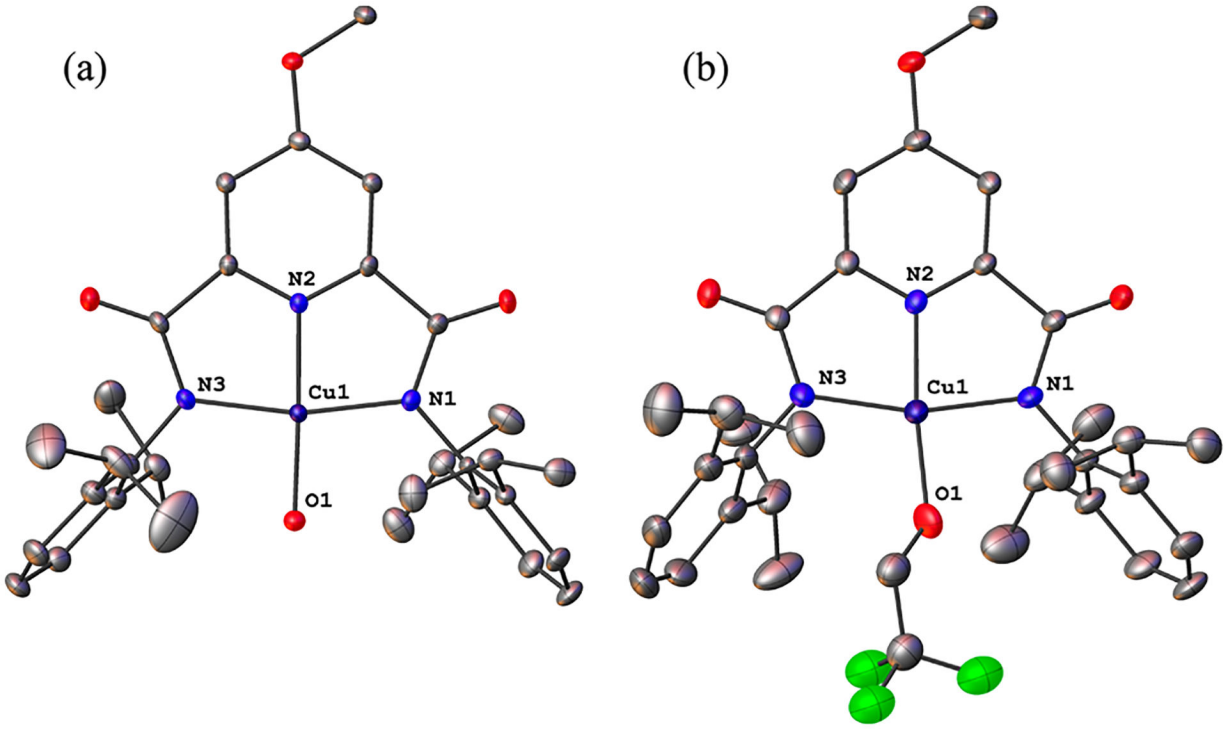

Figure 3.

Representations of the X-ray structures of (a) $L^{OMe}CuOH$ and (b) $L^{OMe}CuOCH_2CF_3$, showing all nonhydrogen atoms as 50% thermal ellipsoids.

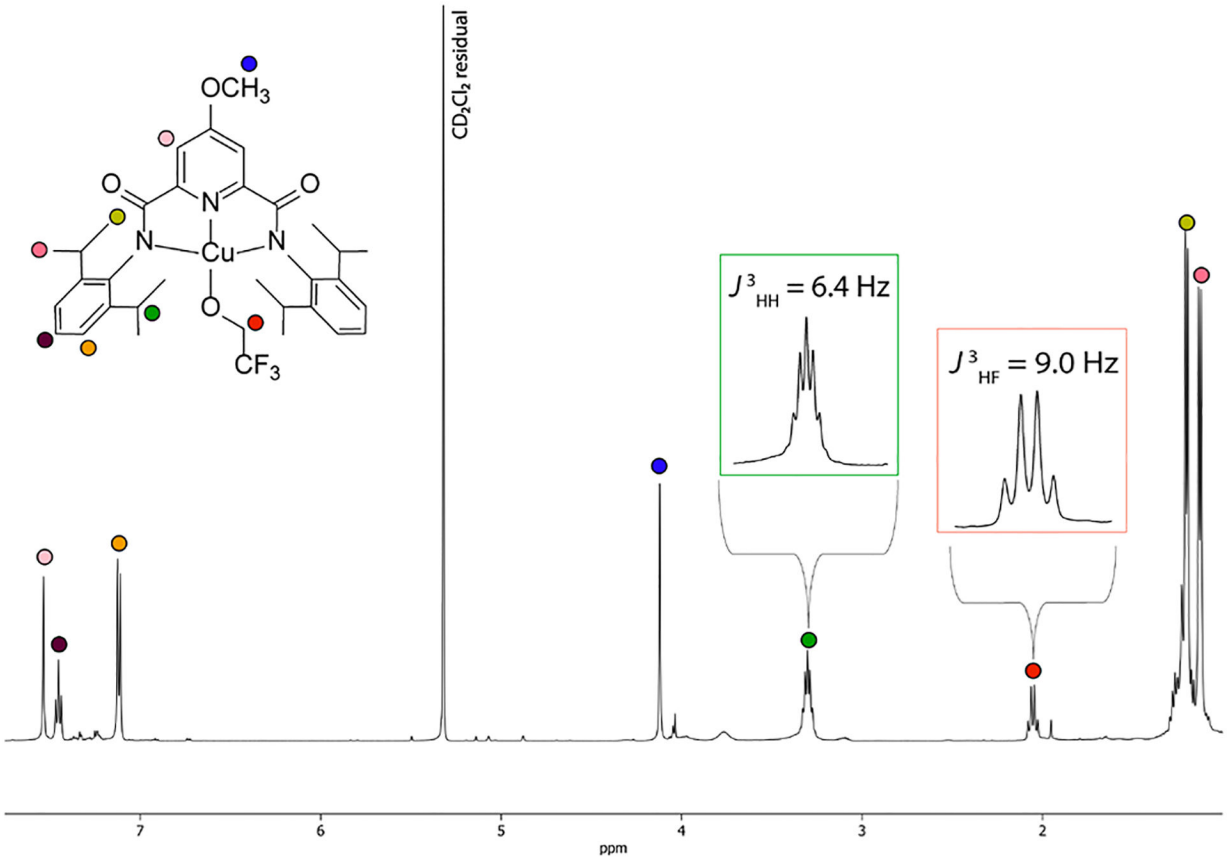

Figure 4.
^{1}H NMR spectrum of $L^{OMe}CuOCH_2CF_3$ (CD_2Cl_2, −15 °C).

Table 1.

Bond Distances (Å) Obtained by X-ray Crystallography for $[CuOR]^{2+}$ (Cu^{III}) and $[CuOR]^{+}$ (Cu^{II}) Species and by DFT Geometry Optimization for $[CuOR]^{2+}$ (Theory)[a]

bond	species	L^{OMe}, OH	L^{H}, OCH_2CF_3	L^{OMe}, OCH_2CF_3
Cu-N_2	Cu^{III}	1.841(3)	1.864(13)	1.856(3)
	theory	*1.845*	*1.875*	*1.866*
	Cu^{II}	1.927(2)	1.925(4)	1.927(1)
	Cu^{III}–Cu^{II}	−0.086	−0.061	−0.071
Cu-$N_{1,3}$	Cu^{III}	1.900(3)	1.950(12)	1.948(3)
	theory	*1.916*	*1.960*	*1.960*
	Cu^{II}	2.027(2)	2.058(4)	2.020(1)
	Cu^{III}–Cu^{II}	−0.127	−0.108	−0.072
Cu-O_1	Cu^{III}	1.799(3)	1.812(12)	1.849(5)
	theory	*1.783*	*1.818*	*1.817*
	Cu^{II}	1.867(2)	1.857(4)	1.838(2)
	Cu^{III}–Cu^{II}	−0.068	−0.045	0.011
mean	Cu^{III}–Cu^{II}	−0.102	−0.081	−0.051

[a]Averaged values are presented for carboxamide Cu–N_1 and Cu–N_3 bonds. N_2 is pyridyl donor. Estimated standard deviations are in parentheses.

Table 2.

Reduction Potentials for the $[CuOR]^{2+/+}$ Couple and Rate Constants for Reactions with ^{ttb}PhOH

compound	$E_{1/2}$ (mV)[a]	k_2 (M^{-1} s^{-1})[b]
$L^{H}CuOH$	−167[c]	15 900
$L^{OMe}CuOH$	−202	11 800
$LCuOCH_2CF_3$	+37	3.0
$L^{OMe}CuOCH_2CF_3$	−25	1.5

[a] Conditions: THF, 0.2 M Bu_4NPF_6, values vs $Fc^{+/0}$.

[b] Conditions: −25 °C in DFB using either 1 equiv ($L^{Y}CuOH$) or 50 equiv ($L^{Y}CuOCH_2CF_3$).

[c] This value is ~100 mV lower than reported previously under the same conditions,[11] which we ascribe to the previous use of external Fc referencing rather than the internal referencing used herein. (See SI IV for details.)